

Dichotomy between in-plane magnetic susceptibility and resistivity anisotropies in extremely strained BaFe_2As_2

Mingquan He,^{1,*} Liran Wang,¹ Felix Ahn,² Frédéric Hardy,¹ Thomas Wolf,¹
Peter Adelman,¹ Jörg Schmalian,^{1,3} Ilya Eremin,² and Christoph Meingast^{1,†}

¹*Institute for Solid State Physics, Karlsruhe Institute of Technology, 76021 Karlsruhe, Germany*

²*Institut für Theoretische Physik III, Ruhr-Universität Bochum, D-44801 Bochum, Germany*

³*Institute for Theory of Condensed Matter, Karlsruhe Institute of Technology, 76131 Karlsruhe, Germany*

(Dated: 10/18/16)

The in-plane resistivity and uniform magnetic susceptibility anisotropies of BaFe_2As_2 are obtained with a new method, in which a large symmetry-breaking uniaxial strain is applied using a substrate with a very anisotropic thermal expansion. The resistivity anisotropy and its corresponding elastoresistivity exhibit very similar diverging behavior as those obtained from piezo-stack experiments. This suggests that the resistivity anisotropy is more a direct measure of magnetism than of nematicity, since the nematic transition is no longer well-defined under a large strain. In strong contrast to the large resistivity anisotropy above T_N , the anisotropy of the in-plane magnetic susceptibility develops largely below T_N . Using an itinerant model, we show that the observed anisotropy ($\chi_b > \chi_a$) is determined by spin-orbit coupling and the orientation of the magnetic moments in the antiferromagnetic phase, and that the anisotropy is dominated by intra-orbital (yz, yz) contributions of the Umklapp susceptibility.

One striking similarity between iron-based superconductors (IBS) and high T_c cuprate superconductors is that superconductivity emerges in close proximity to a magnetic instability [1–3]. Most iron pnictides have a stripe-type antiferromagnetic phase, in which the Fe magnetic moments are parallel to the ordering wave vector either $\mathbf{Q}_1 = (\pi, 0)$ or $\mathbf{Q}_2 = (0, \pi)$, which breaks the C_4 symmetry of the paramagnetic structure [4–7]. The magnetic transition at T_N is accompanied, or sometimes even preceded, by a small orthorhombic structural distortion at $T_S \geq T_N$, which has raised the question of whether magnetism alone is driving these transitions [8–11], or whether orbital degrees of freedom also need to be considered [12–15]. This issue is particularly pressing for FeSe, which has no long-range magnetic order down to the lowest temperature at ambient pressure but nevertheless exhibits a similar orthorhombic distortion as the other Fe-based materials [16–18]. This non-magnetic and orthorhombic phase has been coined ‘electronic nematic’ [10, 19]. Experimentally, the susceptibility to form a nematic state has been probed by a variety of methods, including elastic [20–22], resistivity anisotropy using a piezo stack [23–26], Raman scattering [27–29], thermopower [30], NMR [31, 32], optical conductivity [33, 34]. Interestingly, many optimally doped Fe-based materials appear to be close to a putative nematic quantum critical point [26], and recent theoretical works suggest that electronic nematic fluctuations may provide a boost to superconductivity in various channels [35].

In this Letter we study the interplay between magnetism and nematicity in the parent compound BaFe_2As_2 using a somewhat different approach. Rather than probing the nematic susceptibility in the zero-strain limit, we suppress the nematic transition by imposing a large symmetry breaking strain on the crystal and then examine

the response of both the resistivity anisotropy and the magnetic susceptibility anisotropy. In strong contrast to the large resistivity anisotropy above T_N , the anisotropy of the in-plane magnetic susceptibility develops largely below T_N , although both quantities are to first-order expected to be proportional to the nematic order parameter in the spin-nematic scenario [10, 11]. Further, we show that the resistivity anisotropy exhibits a sharp maximum at T_N and not at T_S , as expected in the spin-nematic picture [10, 11]. Using an itinerant model, we show that the observed anisotropy ($\chi_b > \chi_a$) is determined by spin-orbit coupling and the orientation of the magnetic moments in the antiferromagnetic phase, and that the anisotropy is dominated by intra-orbital (yz, yz) contributions of the Umklapp susceptibility.

Self-flux grown single crystals of BaFe_2As_2 , with typical dimensions of $2 \text{ mm} \times 2 \text{ mm} \times 0.08 \text{ mm}$, were glued onto a glass-fiber reinforced plastic (GFRP) substrate using two-component epoxy (UHU Plus Endfest 300, 90 minutes) with the crystal’s tetragonal $[110]_{\text{tet}}$ direction orientated parallel to the fibers (see Fig. 1(a)). In order to determine the uniaxial strain applied to the sample, the thermal expansion of the GFRP substrate material was characterized by a home-built high resolution capacitance dilatometer [36]. Electrical contacts, with typical resistances of around 2Ω , were made using silver paste, and the sample resistance along two perpendicular directions was measured simultaneously on the same sample by a four-terminal method. Magnetization measurements both parallel and perpendicular to the fiber orientation of the substrate were carried out in a Physical Property Measurement System (PPMS) using the Vibrating Sample Magnetometer (VSM) unit from Quantum Design Inc.

Figure 1(b) shows that the difference of the thermal ex-

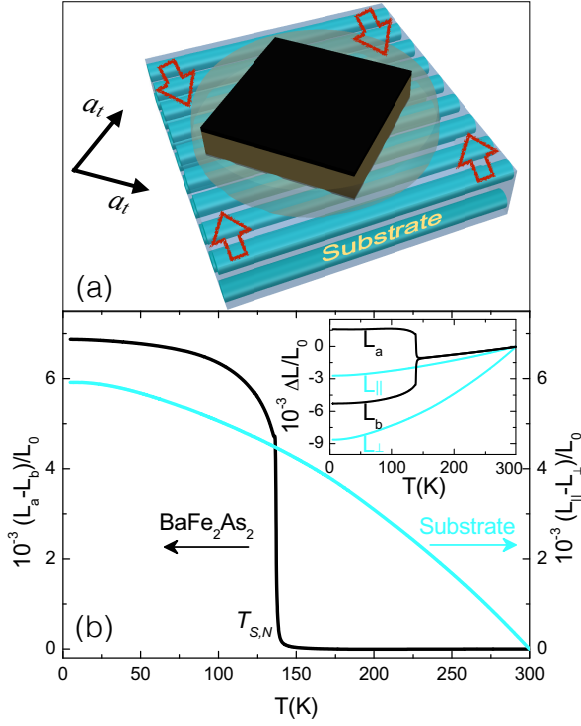


FIG. 1. (a) Illustration of the uniaxial straining set-up. The crystal is glued on top of a glass-fiber reinforced plastic substrate using epoxy with the $[110]_{tet}$ direction parallel to fibers. Upon cooling, the thermal-expansion anisotropy of the substrate applies a uniaxial strain to the crystal. (b) Uniaxial strain of the substrate (L_{\perp} : perpendicular to fibers, L_{\parallel} : parallel to fibers) compared to the in-plane orthorhombic distortion of a free standing BaFe_2As_2 crystal (L_a : longer orthorhombic axis, L_b : shorter orthorhombic axis). The thermal expansion is shown in the inset.

pansion parallel and perpendicular to the fiber direction of the substrate material is comparable in magnitude to the orthorhombic distortion of a free standing BaFe_2As_2 crystal [21, 37] near the transition temperature. Thus, by glueing the BaFe_2As_2 crystal to this substrate at room temperature, a uniaxial symmetry-breaking strain on the order of $\sim 4 \times 10^{-3}$ can be expected at 140 K, which is roughly an order of magnitude larger than the strain applied by the piezo-stack technique [23–26]. As will be shown in the following, our uniaxial straining technique thus allows us to study the response under extreme conditions, and, in particular, allows us to measure both the in-plane resistivity and the uniform magnetic susceptibility anisotropies due to the small size of the setup.

The measured in-plane resistivities of BaFe_2As_2 in the uniaxial-strain setup are shown in Figure 2(a). The resistivities ρ_b and ρ_a were measured on the same sample and are normalized by the resistivity at 300 K in order to eliminate geometrical uncertainties of the contacts. Our in-plane resistivity anisotropy with $\rho_b > \rho_a$ is consistent with the largest anisotropy $(\kappa = \rho_b/\rho_a - 1)_{max} \sim 40\%$ obtained by conventional detwinning methods [38–42],

proving that the sample experiences a large uniaxial strain. A quite high (for BaFe_2As_2) residual resistivity ratio (RRR ~ 10) is found, attesting for the high quality of our crystals. The inset in Fig. 2(a) provides more details near T_N . Both ρ_a and ρ_b exhibit sharp drops at $T = 138.5$ K, which we identify with the magnetic transition, and ρ_b has a maximum about 5 K above the magnetic transition. The m_{66} of the elastoresistivity tensor has proved very useful for studying the nematic susceptibility χ_N [23–26], can also be calculated for our data since we know the applied anisotropic strain from the thermal expansion of the substrate (see Fig. 1). Here,

$$2m_{66}(T) = \frac{\rho_b(T) - \rho_a(T)}{\rho_0(T)(\varepsilon_{\perp}(T) - \varepsilon_{\parallel}(T))},$$

$$\rho_0(T) = \frac{1}{2}[\rho_b(T) + \rho_a(T)]. \quad (1)$$

We find (see Fig. 2(b)) that $|2m_{66}|$ exhibits a very similar magnitude and divergent Curie-Weiss behavior as T_N is approached from above as found in the elastoresistivity data obtained using a piezo-stack, in which a much smaller strain is applied [23–26]. This implies that the resistivity change $\Delta\rho/\rho_0(\varepsilon)$ varies approximately linearly with applied strain ε up to the large strains studied here. Similar to a ferromagnet in an applied field, we no longer expect a real nematic phase transition for the large strain applied here [43], and therefore the observation of a sharp peak in the resistivity anisotropy is quite surprising. Our results thus suggest that the resistivity anisotropy is more directly related to the magnetic transition than to the nematic fluctuations. We note that a similar conclusion can be deduced from the data of Ref. [44], in which the peak in the resistivity anisotropy also occurs at T_N in spite of the fairly large uniaxial pressure applied.

Since the 'detwinning apparatus' in our case is reduced to a thin substrate plate, our method is also feasible for investigating the anisotropy of other quantities, e.g. the magnetization. Fig. 2(c) displays the raw magnetization data at 12 Tesla of a BaFe_2As_2 crystal glued to the glass-fiber substrate in two different orientations (blue and red lines), as well as the bare substrate in the same two orientations (black and green lines). A clear sign of magnetization anisotropy is already observable in the raw data below T_N , despite of a considerable Curie-Weiss component in the magnetization of the GFRP material, which needs to be subtracted. The calculated susceptibility data after subtraction of the substrate background are shown in Fig. 2(d) along with data of a free-standing crystal in the twinned state. Well above T_N , the susceptibilities along both directions are practically identical and decrease linearly with temperature, as previously observed [45] and also exists in other Fe-based systems [46, 47]. Below T_N , the susceptibility along the longer axis χ_a becomes significantly smaller than that of the shorter axis χ_b . The difference between χ_a and χ_b keeps increasing with decreasing temperature and the anisotropic ratio

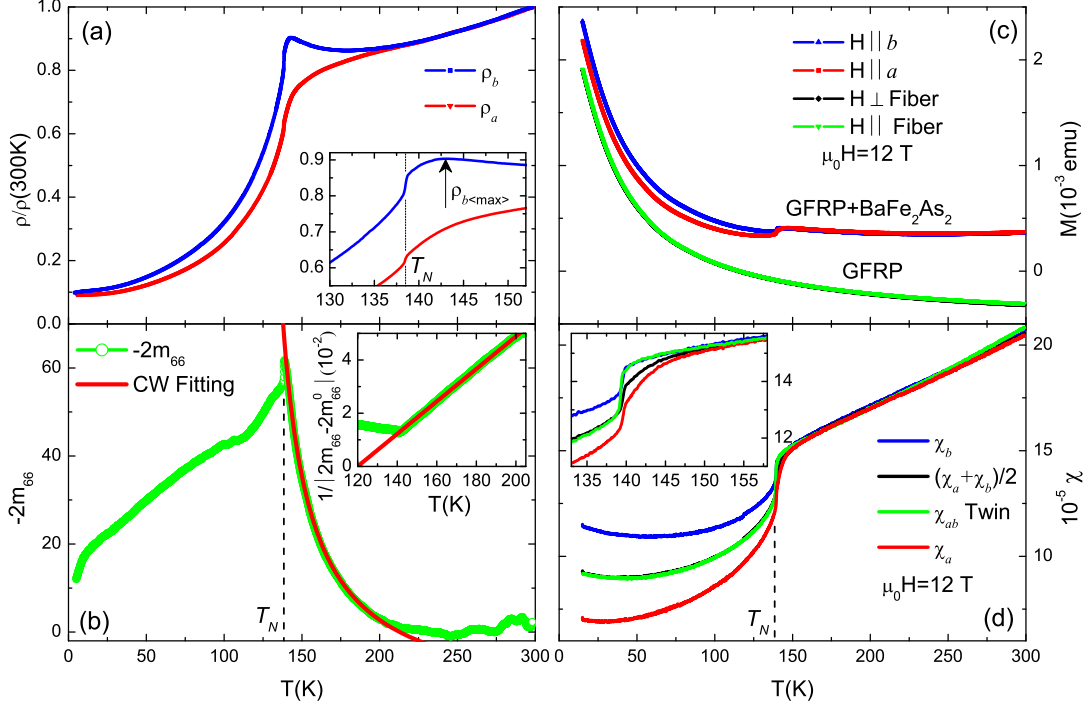


FIG. 2. Temperature dependence of (a) the in-plane resistivity along a and b directions, (b) the elasto-resistivity tensor $2m_{66}$, (c) raw magnetization data of GFRP alone and together with the BaFe_2As_2 crystal, and (d) anisotropic susceptibility obtained by subtracting the GFRP background from the data shown in (c). The red solid line in (b) is a Curie-Weiss fit ($|2m_{66}| = a/(T - T_0) + b$ with $T_0 = 120 \pm 1$ K) and the inset shows the inverse plot. The insets in (a) and (d) display magnified views near T_N . The arrow in the inset of (a) indicates a maximum of ρ_b .

$\eta = \chi_b/\chi_a - 1$ reaches $\sim 60\%$ at 15 K. The average of χ_a and χ_b (black line in Fig. 2(d)) agrees excellently with the twinned data χ_t within the whole temperature range, except slightly above T_N (see inset of Fig. 2(d)), where the averaged data show a significant precursor to the transition starting at about 150 K. We note that the observed sign, $\chi_b > \chi_a$, explains the sign of the magnetic detwinning effect reported in Ref. [48, 49], however we observe no anisotropy at ~ 170 K, as claimed in torque magnetometry experiments on BaFe_2As_2 [50].

Fig. 3 highlights the surprisingly different behavior of the susceptibility anisotropy, $\chi_b - \chi_a$, and the resistivity anisotropy, $\rho_b - \rho_a$. Whereas $\rho_b - \rho_a$ is peaked close to and extends considerably above T_N , $\chi_b - \chi_a$ only starts to develop slightly above T_N and then increases to the lowest temperatures. Thus, the resistivity anisotropy and the susceptibility anisotropy do not scale linearly with each other above the transition, in contrary to the expectation of the spin-nematic scenario [10, 11]. Below we show that this is due to the fact that the susceptibility anisotropy due to the combination of nematic/orbital order and spin-orbit coupling is much weaker than the one caused by the anisotropy due to long range magnetic order. Thus, the combination of susceptibility and resistivity anisotropy can be used to disentangle these two phenomena.

The most natural way to account for the anisotropy of the magnetic susceptibility in the magnetically ordered state is to include spin-orbit coupling in the effective low-energy model of the iron-based superconductors. Indeed, it is responsible for the observed magnetic anisotropy of the striped antiferromagnetic state, namely, for the alignment of the magnetic moments parallel to the AF wave-vector \mathbf{Q}_1 at the transition temperature [51]. We describe

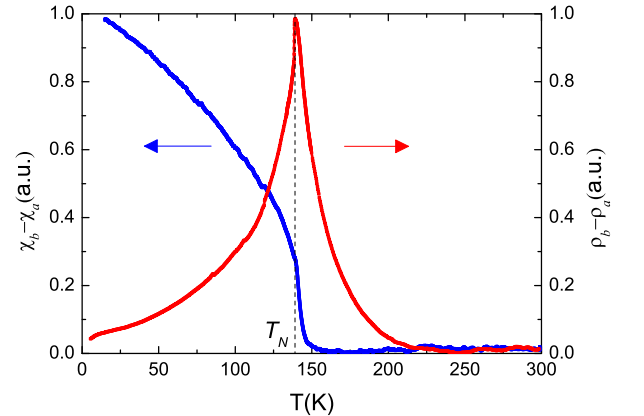


FIG. 3. Temperature dependence of in-plane resistivity and susceptibility anisotropies. Both curves are scaled for clarity.

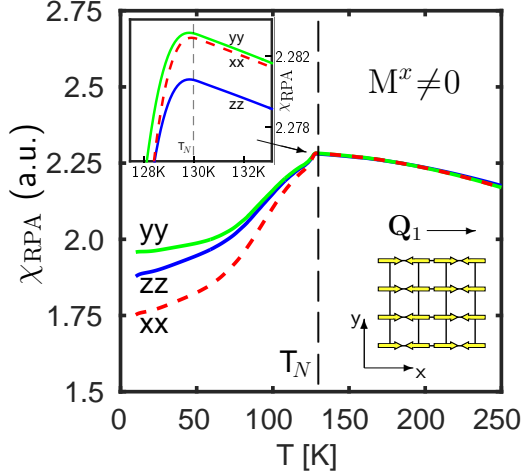


FIG. 4. Magnetic susceptibility calculated in the stripe AF phase using an itinerant multi-orbital model (coordinate basis is transformed as $a \rightarrow x, b \rightarrow y, c \rightarrow z$ in comparison with experimental data). The magnetic moments are arranged parallel to the AF wave vector \mathbf{Q}_1 so that $M^x \neq 0, M^{y,z} = 0$ resulting in $\chi^{yy} > \chi^{xx}$ in agreement with experiment. The inset shows an enlarged view near the transition where an extremely weak splitting ($\ll 1\%$) between χ^{xx} and χ^{yy} occurs in the paramagnetic state due to the finite orbital ordering ($\Delta_{oo} = -25$ meV).

(details can be found in supplemental material [52]) the itinerant electron system of the parent iron-based superconductors by a multi-orbital Hubbard Hamiltonian, which consists of the non-interacting hopping Hamiltonian within the $3d$ -orbital manifold, H_0 , and Hubbard-Hund interaction, H_{int} . We specify the hopping parameters $t_{ij}^{\mu\nu}$ according to the band-structure parametrization obtained by Ikeda [53] for a five orbital model or three-orbital model by Daghofer [54]. Besides the band dispersions, the non-interacting Hamiltonian must also contain the spin orbit coupling term $\lambda \mathbf{S} \cdot \mathbf{L}$ with \mathbf{S} and \mathbf{L} denoting the spin and orbital angular momentum operator, respectively. Note that this atomic-like term preserves the Kramers degeneracy of each state. We project this term from the $L = 2$ spherical harmonic basis to the orbital basis using the standard procedure of Ref. [51]. In order to simulate the breaking of the C_4 symmetry above T_N in the experiment, we also introduced a uniform energy splitting of the d_{xz} and d_{yz} orbitals [55],

$$H_{oo} = \Delta_{oo} \sum_{\mathbf{k}\sigma} (c_{xz\mathbf{k}\sigma}^\dagger c_{xz\mathbf{k}\sigma} - c_{yz\mathbf{k}\sigma}^\dagger c_{yz\mathbf{k}\sigma}), \quad (2)$$

where $\Delta_{oo} = -25$ meV was used so that d_{yz} shifts upwards. Note that such a term appears in the striped AF state automatically as a result of the magnetic ordering breaking the C_4 symmetry of the lattice.

The results of our susceptibility calculations (see supplemental material for details [52]) are shown in Fig. 4. To compare with experimental data, we assign $a \rightarrow$

$x, b \rightarrow y, c \rightarrow z$. As expected, the sign of in-plane susceptibility anisotropy strongly depends on the orientation of the magnetic moments. Alignment of the magnetic moments along \mathbf{Q}_1 driven by spin-orbit coupling produces the anisotropy observed in our magnetization experiments, i.e. $\chi^{yy} > \chi^{xx}$. We note that this is also the same anisotropy expected in a purely localized magnetic model, i.e. the susceptibility is larger for fields perpendicular to the moments. Apart from spin-orbit coupling, the calculation shows that the Umklapp susceptibility dominated by intra-orbital (yz, yz) contributions is responsible for the observed pronounced anisotropy. The inset in Fig. 4 shows that the anisotropy induced by finite orbital ordering in the paramagnetic state is extremely weak $\eta = \chi^{yy}/\chi^{xx} - 1 \ll 1\%$. Orbital ordering therefore can not be responsible for the non-negligible anisotropy slightly above T_N observed in our experimental data. The small effect is however in agreement with the comparatively small orbitally induced susceptibility anisotropy in the wide region between 150 K and 200 K, see Fig. 3.

In summary, we have determined the in-plane resistivity and susceptibility anisotropies of BaFe_2As_2 using a new and simple method, which applies a large uniaxial strain. Interestingly, in spite of the strain-induced 'smearing' of the structural, or nematic transition, the resistivity anisotropy and its corresponding nematic susceptibility show the same behavior as those measured in zero-strain limit, suggesting that the resistivity anisotropy is more directly related to the magnetic transition than to the nematic fluctuations. The observed susceptibility anisotropy in the magnetically ordered phase qualitatively agrees well with calculations using an effective low-energy itinerant model including spin-orbit coupling, in which the sizable splitting is dominated by intra-orbital (yz, yz) Umklapp processes. Striking is the different behavior of the resistivity and susceptibility anisotropies in the paramagnetic uniaxially strained state. In particular, whereas the resistivity anisotropy exhibits a Curie-Weiss divergence extending to temperatures much larger than T_N , the susceptibility anisotropy develops only about 10 K above T_N . Our calculations show that orbital order produces a negligible susceptibility anisotropy above T_N and serve to disentangle anisotropies due to orbital and nematic order from those of the magnetically ordered state.

We thank Rafael Fernandes and Igor Mazin for valuable discussions.

* mingquan.he@kit.edu

† christoph.meingast@kit.edu

- [1] K. Ishida, Y. Nakai, and H. Hosono, *J. Phys. Soc. Jpn.* **78**, 062001 (2009).
- [2] D. C. Johnston, *Adv. Phys.* **59**, 803 (2010).

- [3] P. J. Hirschfeld, M. M. Korshunov, and I. I. Mazin, *Rep. Prog. Phys.* **74**, 124508 (2011).
- [4] K. Kitagawa, N. Katayama, K. Ohgushi, M. Yoshida, and M. Takigawa, *J. Phys. Soc. Jpn.* **77**, 114709 (2008).
- [5] Q. Huang, Y. Qiu, W. Bao, M. A. Green, J. W. Lynn, Y. C. Gasparovic, T. Wu, G. Wu, and X. H. Chen, *Phys. Rev. Lett.* **101**, 257003 (2008).
- [6] P. Dai, J. Hu, and E. Dagotto, *Nat. Phys.* **8**, 709 (2012).
- [7] P. Dai, *Rev. Mod. Phys.* **87**, 855 (2015).
- [8] C. Fang, H. Yao, W.-F. Tsai, J. Hu, and S. A. Kivelson, *Phys. Rev. B* **77**, 224509 (2008).
- [9] S. Nandi, M. G. Kim, A. Kreyssig, R. M. Fernandes, D. K. Pratt, A. Thaler, N. Ni, S. L. Bud'ko, P. C. Canfield, J. Schmalian, R. J. McQueeney, and A. I. Goldman, *Phys. Rev. Lett.* **104**, 057006 (2010).
- [10] R. M. Fernandes and J. Schmalian, *Supercond. Sci. Technol* **25**, 084005 (2012).
- [11] R. M. Fernandes, A. V. Chubukov, and J. Schmalian, *Nat. Phys.* **10**, 97 (2014).
- [12] F. Krüger, S. Kumar, J. Zaanen, and J. van den Brink, *Phys. Rev. B* **79**, 054504 (2009).
- [13] H. Kontani and S. Onari, *Phys. Rev. Lett.* **104**, 157001 (2010).
- [14] H. Kontani, T. Saito, and S. Onari, *Phys. Rev. B* **84**, 024528 (2011).
- [15] H. Yamase and R. Zeyher, *Phys. Rev. B* **88**, 180502 (2013).
- [16] F.-C. Hsu, J.-Y. Luo, K.-W. Yeh, T.-K. Chen, T.-W. Huang, P. M. Wu, Y.-C. Lee, Y.-L. Huang, Y.-Y. Chu, D.-C. Yan, and M.-K. Wu, *Proc. Natl. Acad. Sci. U.S.A.* **105**, 14262 (2008).
- [17] T. M. McQueen, A. J. Williams, P. W. Stephens, J. Tao, Y. Zhu, V. Ksenofontov, F. Casper, C. Felser, and R. J. Cava, *Phys. Rev. Lett.* **103**, 057002 (2009).
- [18] A. E. Böhmer, F. Hardy, F. Eilers, D. Ernst, P. Adelmann, P. Schweiss, T. Wolf, and C. Meingast, *Phys. Rev. B* **87**, 180505 (2013).
- [19] E. Fradkin, S. A. Kivelson, M. J. Lawler, J. P. Eisenstein, and A. P. Mackenzie, *Annu. Rev. Condens. Matter Phys.* **1**, 153 (2010).
- [20] A. E. Böhmer, P. Burger, F. Hardy, T. Wolf, P. Schweiss, R. Fromknecht, M. Reinecker, W. Schranz, and C. Meingast, *Phys. Rev. Lett.* **112**, 047001 (2014).
- [21] A. E. Böhmer, F. Hardy, L. Wang, T. Wolf, P. Schweiss, and C. Meingast, *Nat. Commun.* **6**, 7911 (2015).
- [22] A. E. Böhmer and C. Meingast, *Comptes Rendus Physique* **17**, 90 (2016).
- [23] J.-H. Chu, H.-H. Kuo, J. G. Analytis, and I. R. Fisher, *Science* **337**, 710 (2012).
- [24] H.-H. Kuo, M. C. Shapiro, S. C. Riggs, and I. R. Fisher, *Phys. Rev. B* **88**, 085113 (2013).
- [25] H.-H. Kuo and I. R. Fisher, *Phys. Rev. Lett.* **112**, 227001 (2014).
- [26] H.-H. Kuo, J.-H. Chu, J. C. Palmstrom, S. A. Kivelson, and I. R. Fisher, *Science* **352**, 958 (2016).
- [27] Y. Gallais, R. M. Fernandes, I. Paul, L. Chauvière, Y.-X. Yang, M.-A. Méasson, M. Cazayous, A. Sacuto, D. Colson, and A. Forget, *Phys. Rev. Lett.* **111**, 267001 (2013).
- [28] Y. Gallais and I. Paul, *Comptes Rendus Physique* **17**, 113 (2016).
- [29] F. Kretschmar, T. Böhm, U. Karahasanovic, B. Muschler, A. Baum, D. Jost, J. Schmalian, S. Caprara, M. Grilli, C. Di Castro, J. G. Analytis, J. H. Chu, I. R. Fisher, and R. Hackl, *Nat. Phys.* **12**, 560 (2016).
- [30] S. Jiang, H. S. Jeevan, J. Dong, and P. Gegenwart, *Phys. Rev. Lett.* **110**, 067001 (2013).
- [31] M. Fu, D. A. Torchetti, T. Imai, F. L. Ning, J.-Q. Yan, and A. S. Sefat, *Phys. Rev. Lett.* **109**, 247001 (2012).
- [32] T. Iye, M.-H. Julien, H. Mayaffre, M. Horvatić, C. Berthier, K. Ishida, H. Ikeda, S. Kasahara, T. Shibauchi, and Y. Matsuda, *J. Phys. Soc. Jpn.* **84**, 043705 (2015).
- [33] M. Nakajima, T. Liang, S. Ishida, Y. Tomioka, K. Kihou, C. H. Lee, A. Iyo, H. Eisaki, T. Kakeshita, T. Ito, and S. Uchida, *Proc. Natl. Acad. Sci. U.S.A.* **108**, 12238 (2011).
- [34] A. Dusza, A. Lucarelli, F. Pfanner, J.-H. Chu, I. R. Fisher, and L. Degiorgi, *Europhys. Lett.* **93**, 37002 (2011).
- [35] S. Lederer, Y. Schattner, E. Berg, and S. A. Kivelson, *Phys. Rev. Lett.* **114**, 097001 (2015).
- [36] C. Meingast, B. Blank, H. Bürkle, B. Obst, T. Wolf, H. Wühl, V. Selvamannickam, and K. Salama, *Phys. Rev. B* **41**, 11299 (1990).
- [37] L. Wang, F. Hardy, A. E. Böhmer, T. Wolf, P. Schweiss, and C. Meingast, *Phys. Rev. B* **93**, 014514 (2016).
- [38] J.-H. Chu, J. G. Analytis, K. De Greve, P. L. McMahon, Z. Islam, Y. Yamamoto, and I. R. Fisher, *Science* **329**, 824 (2010).
- [39] S. Ishida, M. Nakajima, T. Liang, K. Kihou, C. H. Lee, A. Iyo, H. Eisaki, T. Kakeshita, Y. Tomioka, T. Ito, and S. Uchida, *Phys. Rev. Lett.* **110**, 207001 (2013).
- [40] M. A. Tanatar, E. C. Blomberg, A. Kreyssig, M. G. Kim, N. Ni, A. Thaler, S. L. Bud'ko, P. C. Canfield, A. I. Goldman, I. I. Mazin, and R. Prozorov, *Phys. Rev. B* **81**, 184508 (2010).
- [41] J. J. Ying, X. F. Wang, T. Wu, Z. J. Xiang, R. H. Liu, Y. J. Yan, A. F. Wang, M. Zhang, G. J. Ye, P. Cheng, J. P. Hu, and X. H. Chen, *Phys. Rev. Lett.* **107**, 067001 (2011).
- [42] E. C. Blomberg, M. A. Tanatar, R. M. Fernandes, I. I. Mazin, B. Shen, H.-H. Wen, M. D. Johannes, J. Schmalian, and R. Prozorov, *Nat. Commun.* **4**, 1914 (2013).
- [43] R. M. Fernandes, E. Abrahams, and J. Schmalian, *Phys. Rev. Lett.* **107**, 217002 (2011).
- [44] H. Man, X. Lu, J. S. Chen, R. Zhang, W. Zhang, H. Luo, J. Kulda, A. Ivanov, T. Keller, E. Morosan, Q. Si, and P. Dai, *Phys. Rev. B* **92**, 134521 (2015).
- [45] X. F. Wang, T. Wu, G. Wu, H. Chen, Y. L. Xie, J. J. Ying, Y. J. Yan, R. H. Liu, and X. H. Chen, *Phys. Rev. Lett.* **102**, 117005 (2009).
- [46] G. M. Zhang, Y. H. Su, Z. Y. Lu, Z. Y. Weng, D. H. Lee, and T. Xiang, *Europhys. Lett.* **86**, 37006 (2009).
- [47] R. Klingeler, N. Leps, I. Hellmann, A. Popa, U. Stockert, C. Hess, V. Kataev, H.-J. Grafe, F. Hammerath, G. Lang, S. Wurmehl, G. Behr, L. Harnagea, S. Singh, and B. Büchner, *Phys. Rev. B* **81**, 024506 (2010).
- [48] J.-H. Chu, J. G. Analytis, D. Press, K. De Greve, T. D. Ladd, Y. Yamamoto, and I. R. Fisher, *Phys. Rev. B* **81**, 214502 (2010).
- [49] S. Zapf, C. Stingl, K. W. Post, J. Maiwald, N. Bach, I. Pietsch, D. Neubauer, A. Löhle, C. Clauss, S. Jiang, H. S. Jeevan, D. N. Basov, P. Gegenwart, and M. Dressel, *Phys. Rev. Lett.* **113**, 227001 (2014).
- [50] S. Kasahara, H. J. Shi, K. Hashimoto, S. Tonegawa, Y. Mizukami, T. Shibauchi, K. Sugimoto, T. Fukuda, T. Terashima, A. H. Nevidomskyy, and Y. Matsuda, *Nature* **486**, 382 (2012).

- [51] M. H. Christensen, J. Kang, B. M. Andersen, I. Eremin, and R. M. Fernandes, [Phys. Rev. B **92**, 214509 \(2015\)](#).
- [52] See Supplemental Material at URL will be inserted by publisher for calculation details.
- [53] H. Ikeda, R. Arita, and J. Kuneš, [Phys. Rev. B **81**, 054502 \(2010\)](#).
- [54] M. Daghofer, A. Nicholson, A. Moreo, and E. Dagotto, [Phys. Rev. B **81**, 014511 \(2010\)](#).
- [55] R. M. Fernandes and O. Vafek, [Phys. Rev. B **90**, 214514 \(2014\)](#).

I. Supplemental Material: Dichotomy between in-plane magnetic susceptibility and resistivity anisotropies in extremely strained BaFe₂As₂

The itinerant electron system of the parent iron-based superconductors can be described by a multi-orbital Hubbard Hamiltonian, which consists of the non-interacting hopping Hamiltonian within the 3d-orbital manifold, H_0 , and the Hubbard-Hund interaction, H_{int} ,

$$H = H_0 + H_{\text{int}}, \quad (1)$$

with

$$H_0 = \sum_{\sigma} \sum_{i,j} \sum_{\mu,\nu} c_{i\mu\sigma}^{\dagger} (t_{ij}^{\mu\nu} - \mu_0 \delta_{ij} \delta_{\mu\nu}) c_{j\nu\sigma}, \quad (2)$$

and

$$\begin{aligned} H_{\text{int}} = & U \sum_{i,\mu} n_{i\mu\uparrow} n_{i\mu\downarrow} + U' \sum_{i,\mu<\nu,\sigma} n_{i\mu\sigma} n_{i\nu\sigma} + \\ & (U' - J) \sum_{i,\mu<\nu,\sigma} n_{i\mu\sigma} n_{i\nu\sigma} + \\ & J \sum_{i,\mu<\nu,\sigma} c_{i\mu\sigma}^{\dagger} c_{i\nu\sigma}^{\dagger} c_{i\mu\sigma} c_{i\nu\sigma} + \\ & J' \sum_{i,\mu<\nu,\sigma} c_{i\mu\sigma}^{\dagger} c_{i\mu\sigma}^{\dagger} c_{i\nu\sigma} c_{i\nu\sigma}. \end{aligned} \quad (3)$$

The indices $\mu, \nu \in \{d_{xz}, d_{yz}, d_{x^2-y^2}, d_{xy}, d_{3z^2-r^2}\}$ specify the 3d-Fe orbitals and i, j run over the sites of the square lattice. The doping is fixed by the chemical potential μ_0 . The interactions are parametrized by an intra-orbital on-site Hubbard- U , an inter-orbital coupling U' , Hund's coupling J and pair hopping J' . We employ $U' = U - 2J$, $J = J'$ and set $J = U/4$. The fermionic operators $c_{i\mu\sigma}^{\dagger}$, $c_{i\mu\sigma}$ are the creation and annihilation operators, respectively. We specify the hopping parameters $t_{ij}^{\mu\nu}$ according to the band structure obtained by Ikeda *et al.* [1] or Daghofer *et al.* [2] for the five or three orbital models, respectively.

The approximate nesting between hole pockets around Γ and M and electron pockets around X and Y promotes strong fluctuations in the particle-hole channel at wave vectors $\mathbf{Q}_1 = (\pi, 0)$ and $\mathbf{Q}_2 = (0, \pi)$. The electronic states at the Fermi level are dominated by the d_{xz} , d_{yz} and d_{xy} orbitals, as shown in Fig. S1. While the hole-pockets centered around Γ are formed by d_{xz} and d_{yz} orbitals, the hole pocket at M is mainly of d_{xy} character. The electron pockets at X and Y feature a mixed orbital character, where the inner part facing towards the BZ center is d_{xy} dominated, and the outer parts are d_{yz} and d_{xz} dominated around $(\pi, 0)$ and $(0, \pi)$, respectively. This allows for the further reduction of the 5-orbital model to the three-orbital model only [2].

This directionality of the SDW order parameter, on top of the breaking of rotational symmetry in spin

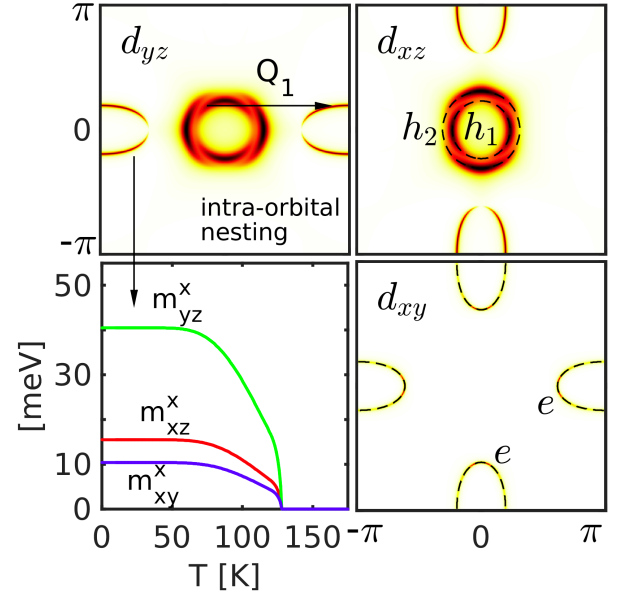


FIG. S1. Typical distribution of the orbital content at the Fermi surface for the iron-based compounds [1, 2]. For the wave-vector \mathbf{Q}_1 , the intra-orbital nesting of the d_{yz} -orbitals dominates over the other orbitals contributions. As a direct consequence, the SDW gap (bottom left corner) and the magnetic Umklapp susceptibility will acquire the largest contribution due the d_{yz} -orbital. The magnetization of the other two orbitals, present at the Fermi level, is mainly induced by the Hund coupling J . Here, m_i^x corresponds to the magnetization of the $l = yz, xz, xy$ orbital along the spin orientation $i = x, y, z$.

space, also breaks the C_4 symmetry of the five orbital model down to a C_2 symmetry. The two different, orbitally resolved SDW order parameters read as $\mathbf{M}_1^{\mu\nu} = \frac{1}{\mathcal{N}} \sum_{\mathbf{k}, \sigma, \sigma'} \langle c_{\mathbf{k}+\mathbf{Q}_1\mu\sigma}^{\dagger} \sigma_{\sigma\sigma'} c_{\mathbf{k}\nu\sigma'} \rangle$, and $\mathbf{M}_2^{\mu\nu} = \frac{1}{\mathcal{N}} \sum_{\mathbf{k}, \sigma, \sigma'} \langle c_{\mathbf{k}+\mathbf{Q}_2\mu\sigma}^{\dagger} \sigma_{\sigma\sigma'} c_{\mathbf{k}\nu\sigma'} \rangle$, with \mathcal{N} the number of unit cells and σ the vector of Pauli matrices. Here, the fermionic creation and annihilation operators for orbital Bloch states with wave vector \mathbf{k} are defined as $c_{\mathbf{k}\mu\sigma}^{\dagger} = \frac{1}{\sqrt{\mathcal{N}}} \sum_i e^{-i\mathbf{k}\cdot\mathbf{r}_i} c_{i\mu\sigma}^{\dagger}$, $c_{\mathbf{k}\mu\sigma} = \frac{1}{\sqrt{\mathcal{N}}} \sum_i e^{i\mathbf{k}\cdot\mathbf{r}_i} c_{i\mu\sigma}$. Taking the orbital trace yields the magnetic moments $\mathbf{M}_1, \mathbf{M}_2$ of the two SDW configurations.

Besides the band dispersions, the non-interacting Hamiltonian must also contain the SOC term $\lambda \mathbf{S} \cdot \mathbf{L}$, with \mathbf{S} denoting the spin angular momentum operator and \mathbf{L} , the orbital angular momentum operator, projected from the $L = 2$ cubic harmonic basis to the orbital basis [3]. Furthermore, in the following we assume that the system possesses a striped AF order with \mathbf{Q}_1 ordering wave-vector and the magnetic moment is pointing along the ordering momentum, i.e. x -direction. Such an order appears to be the ground state for zero doping in several studies of the typical models of the iron-based superconductors [3, 4]. To understand the origin of anisotropy in the uniform susceptibility in the magnetic state, we

note that the magnetic inter-orbital components of the mean-field magnetizations for the C_2 phase were found to be negligible compared to the intra-orbital terms [4]. Furthermore, as mentioned above there are three orbitals contributing to the Fermi surfaces, however, only one of them has a significant portion of the intra-orbital nesting.

As a result the magnetization for the striped antiferromagnetic state with \mathbf{Q}_1 wave vector has largest contribution that arises from the yz -orbital, as shown in Fig. S1.

Next we compute the components of the magnetic susceptibility $\chi_0^{xx/yy/zz}$ in the multi-orbital case,

$$\chi_0^{uu}(\mathbf{q}, \omega) = - \sum_{\mathbf{k}ij} \eta^{uu}(i, \mathbf{k}; j, \mathbf{k} + \mathbf{q}) \times \frac{f(E_j(\mathbf{k} + \mathbf{q})) - f(E_i(\mathbf{k}))}{E_j(\mathbf{k} + \mathbf{q}) - E_i(\mathbf{k}) + \omega + i0^+}, \quad u = x, y, z, \quad (4)$$

which includes the tensor

$$[\eta^{uv}(i, \mathbf{k}; j, \mathbf{k} + \mathbf{q})]_{q\beta, p\alpha}^{s\gamma, t\delta} = \sigma_{\alpha\beta}^u \sigma_{\gamma\delta}^v \times a_{q\beta}(i, \mathbf{k}) a_{s\gamma}^*(i, \mathbf{k}) a_{t\delta}(j, \mathbf{k} + \mathbf{q}) a_{p\alpha}^*(j, \mathbf{k} + \mathbf{q}), \quad (5)$$

expressed with the help of the Pauli matrices σ^u and the elements of the unitary transformations from the band to the orbital basis, a . The physical susceptibility is then obtained by taking the trace over $p = q$ and $s = t$ orbitals.

It is straightforward to show that the anisotropy of the susceptibility enters through the orbital-dressing factors (5) and presence of the Umklapp terms in the antiferro-

magnetic translational-symmetry broken state. We find for the bare susceptibility:

$$\begin{aligned} \chi_0^{xx}(\mathbf{Q}, \omega) &= \text{bubble}_1 + \text{bubble}_2 + \text{bubble}_3 + \text{bubble}_4 \\ \chi_0^{yy}(\mathbf{Q}, \omega) &= \text{bubble}_1 + \text{bubble}_2 - \text{bubble}_3 - \text{bubble}_4 \\ \chi_0^{zz}(\mathbf{Q}, \omega) &= \text{bubble}_1 + \text{bubble}_2 - \text{bubble}_3 - \text{bubble}_4 \end{aligned} \quad (6)$$

Note that in the paramagnetic state and for vanishing spin-orbit coupling, the first two bubbles of each component are equal while the last two Umklapp terms vanish, ensuring the overall $O(3)$ symmetry of the system. If spin-orbit coupling is finite, we find $\chi^{yy} > \chi^{xx,zz}$ at $\mathbf{Q}_1 = (\pi, 0)$ so that an alignment of the magnetic moments parallel to \mathbf{Q}_1 is favored ($M^x \neq 0, M^{y,z} = 0$).

Although spin-orbit coupling is large enough to lower the symmetry by favoring M^x over M^y for the AF wave-vector \mathbf{Q}_1 , it is not large enough to account for the size of the in-plane anisotropy observed below the AF transition temperature. In the following we show that the in-plane splitting of the uniform susceptibility is caused by the intra-orbital Umklapp terms of the yz orbital (xz respectively for \mathbf{Q}_2). In particular, looking at the Eq.(6), one sees that the difference of the two in-plane components originates from the third and fourth bubble diagrams due to the different sign for χ^{xx} and χ^{yy} ,

$$G_{yz, \sigma; yz, \bar{\sigma}}(i, \mathbf{k}) G_{yz, \sigma; yz, \bar{\sigma}}(j, \mathbf{k} + \mathbf{Q}_1). \quad (7)$$

Evaluating the sums we find for the splitting

$$[\chi_0^{xx} - \chi_0^{yy}]_{(\mathbf{q}=0)} = 4 \left[(m_{yz}^x)^2 - (m_{yz}^y)^2 \right] \sum_{i\mathbf{k}} |a_{yz\uparrow}(h_i, \mathbf{k})|^4 |a_{yz\downarrow}(e, \mathbf{k} + \mathbf{Q}_1)|^4 \frac{f(E_i(\mathbf{k})) - f(E_e(\mathbf{k} + \mathbf{Q}_1))}{[E_i(\mathbf{k}) - E_e(\mathbf{k} + \mathbf{Q}_1)]^3} \quad (8)$$

where we have set $\omega = 0$ and denote m_l^i to be the magnetization of the $l = yz, xz, xy$ orbital along the spin orientation $i = x, y, z$. As one clearly sees in the stripe AF phase with ordering momentum \mathbf{Q}_1 with spins aligned either parallel or antiparallel to the x -direction ($M^x \neq 0, m_{yz}^x \neq 0$), both transverse components of the susceptibility split and one has $\chi_0^{yy}(\mathbf{q} = 0, \omega = 0) > \chi_0^{xx}(\mathbf{q} = 0, \omega = 0)$. Furthermore, the sign of the anisotropy is reversed ($M^y \neq 0, m_{yz}^y \neq 0$) if the moments would be pointing out perpendicular to the ordering wave vector. In simple terms the largest AF gap in the spin subspace reduces the corresponding component of the uniform susceptibility.

Our analytical results for the yz orbitals are fully confirmed by the full numerical calculations using the realistic tight-binding models [1, 2]. In particular, in Fig. 4 of the main text we show the calculated uniform susceptibility splitting calculated within random phase approximation. In addition, the numerical study confirms that the in-plane anisotropy is determined by the Umklapp susceptibility involving yz and that the sign of the anisotropy depends on the orientation of the magnetic moments.

Finally we note by passing that the origin of the magnetic anisotropy in the uniform susceptibility cannot be due to the simple ferro-orbital ordering ($n_{xz} - n_{yz} \neq 0$),

introduced by the structural (nematic) transition at $T_S > T_N$ although it breaks the anisotropy between the x and the y component of the spin susceptibility. One finds in this case that the splitting will be proportional to $\Delta_{\text{oo}}\lambda^2$ and thus its sign is reversed as compared to the effect of the magnetic ordering.

* mingquan.he@kit.edu

[†] christoph.meingast@kit.edu

- [1] H. Ikeda, R. Arita, and J. Kuneš, *Phys. Rev. B* **81**, 054502 (2010).
- [2] M. Daghofer, A. Nicholson, A. Moreo, and E. Dagotto, *Phys. Rev. B* **81**, 014511 (2010).
- [3] M. H. Christensen, J. Kang, B. M. Andersen, I. Eremin, and R. M. Fernandes, *Phys. Rev. B* **92**, 214509 (2015).
- [4] M. N. Gastiasoro, I. Paul, Y. Wang, P. J. Hirschfeld, and B. M. Andersen, *Phys. Rev. Lett.* **113**, 127001 (2014).